

# Lateral molecular interaction on heterogeneous surfaces experimentally measured

N.A. Katsanos<sup>a,\*</sup>, F. Roubani-Kalantzopoulou<sup>b</sup>, E. Iliopoulou<sup>a</sup>, I. Bassiotis<sup>b</sup>,  
V. Siokos<sup>b</sup>, M.N. Vrahatis<sup>c</sup>, V.P. Plagianakos<sup>c</sup>

<sup>a</sup> Physical Chemistry Laboratory, University of Patras, 265 04 Patras, Greece

<sup>b</sup> Department of Chemical Engineering, National Technical University, 157 80 Zografou, Greece

<sup>c</sup> Department of Mathematics, University of Patras, 265 04 Patras, Greece

Received 14 May 2001; accepted 7 August 2001

## Abstract

Using inverse gas chromatography, the added to  $\varepsilon$  differential energy of adsorption due to lateral interactions of molecules adsorbed on a heterogeneous solid surface was determined. The method was applied to three gas/solid systems, namely, 1-butene/cadmium sulphide, ethane/calcium oxide, and *trans*-2-butene/marble. By plotting the dimensionless lateral interaction energy against time  $t$  in parallel with the energy distribution function against  $\varepsilon$  and  $t$ , the appearance of curves against  $t$  is quite similar in all three systems. This was explained on the basis of Bakaev and Steele model for adsorption sites, i.e. on the existence of three kinds of sites. © 2002 Elsevier Science B.V. All rights reserved.

**Keywords:** Adsorption isotherms; Atom–solid interactions; Surface energy; Physical adsorption

## 1. Introduction

One is impressed by the various ways used to overcome the difficulty or rather impossibility to obtain an analytical solution of the classical integral equation

$$\Theta(p, T) = \int_0^{\infty} \theta_i(p, T, \varepsilon) f(\varepsilon) d\varepsilon$$

describing adsorption of gases on heterogeneous

surfaces. Any two of the functions  $\Theta$  (experimental adsorption isotherm),  $\theta_i$  (unknown local isotherm), and  $f(\varepsilon)$  (unknown distribution function of the adsorption energy  $\varepsilon$ ) are needed to calculate the remaining one, as described in two well-known books [1,2]. Recently [3–6], however, the above integral equation was circumvented altogether, and only a model for  $\theta_i(p, T, \varepsilon)$  was adopted, namely, the fairly general isotherm of Jovanovic, to calculate the local adsorption energies,  $\varepsilon$ , the local monolayer capacities,  $c_{\max}^*$ , the values of  $\theta_i(p, T, \varepsilon)$ , and the values of  $f(\varepsilon)$ , all as a function of time,  $t$ , directly from experimental data. These data were obtained by

\* Corresponding author. Fax: +30-61-997-110.

E-mail address: [rita@chemistry.upatras.gr](mailto:rita@chemistry.upatras.gr) (N.A. Katsanos).

the inverse gas chromatography technique known as Reversed-Flow Gas Chromatography (RF-GC) [7].

In the present work the same methodology was adopted to calculate as a function of time the energy involved in lateral interactions for pairs of molecules on the solid surface, and its connection with the adsorption energy distribution. The systems used as examples of the calculations were 1-butene/cadmium sulphide, ethane/calcium oxide, and *trans*-2-butene/marble.

## 2. Experimental

The experimental arrangement for the measurements has been described in previous publications [3–5,8,9], and in a recent review [10]. The carrier gas (pure nitrogen dried with silica gel or 13X molecular sieve) is running through the so-called *sampling column* (ca. 120 cm × 4 mm ID stainless steel tube) with a flow-rate of 20–30 cm<sup>3</sup> min<sup>-1</sup>. At about the middle of the sampling column a glass tube (28–43 cm × 4 mm ID) is connected perpendicularly, having its longer part  $L_1$  (23–35 cm) empty (*diffusion column*) and its smaller part  $L_2$  (5–8 cm) filled with 0.5–1 g of the granular solid adsorbent (*solid bed*). The other end of  $L_2$  part is sealed by means of an injector septum. The experimental procedure starts with the injection of a small volume (0.5–1 cm<sup>3</sup> at atmospheric pressure) of the adsorbate gas through the septum onto the solid bed. No carrier gas is running through the glass tube  $L_1 + L_2$ , although this is continually filled with a stagnant volume of it.

The adsorbate injection is followed by repeated flow reversals of short duration (10–60 s) of the carrier gas flowing only through the sampling column. This is easily done by means of a four-port gas valve connecting the one end of the sampling column to the inlet of the carrier gas, and the other end to the detector system. The flow-reversals create narrow fairly symmetrical *sample peaks* being recorded, with their height  $H$  or their area under the curve calculated and printed, together with the corresponding time  $t$ , by a suitable chromatographic

processor. Examples of such sample peaks one can find in Figure 2 of [13].

The 1-butene (1-C<sub>4</sub>H<sub>8</sub>), and the ethane (C<sub>2</sub>H<sub>6</sub>) were obtained from Air Liquide (Athens, Greece). Both had a purity of 99.000–99.999%. The *trans*-2-butene was a Matheson Gas Product of Research Grade. The nitrogen carrier gas was obtained from Linde (99.99% N<sub>2</sub>). The cadmium sulphide (CdS) was a Merck product of analytical grade. The calcium oxide (CaO) was a product of FLUKA (97%), and the CaCO<sub>3</sub> was a Penteli marble (Athens, Greece).

## 3. Theoretical

All calculations in the new method mentioned above are based on the series of the *sample peaks* of considerable height  $H$  ‘sitting’ on the otherwise continuous asymmetric signal. The mathematical equation describing the dependence of  $H$  on time  $t$  has been derived and published [8–10]:

$$H^{1/M} = \sum_{i=1}^4 A_i \exp(B_i t) \quad (1)$$

It describes the so-called *diffusion band* of the RF-GC method,  $M$  denoting the response factor of the chromatographic detector, and  $A_i$ ,  $B_i$  being functions of the physicochemical quantities pertaining to the adsorption phenomena due to a gas adsorbed on the heterogeneous surface of a solid adsorbent. By using non-linear least-squares regression analysis [8–10], one can calculate from the values of the experimental pairs  $H$ ,  $t$  the values of  $A_i$ , and  $B_i$  of Eq. (1). From these, combined with the corrected linear flow velocity  $v$  (cm s<sup>-1</sup>) of the carrier gas, the length  $L_1$  (cm) of the empty diffusion cylindrical column, the cross-sectional area  $a_y$  (cm<sup>2</sup>) of the void space in the solid bed  $L_2$  (placed in continuation of the diffusion column), and the amount of solid per unit length of  $L_2$ ,  $a_s$  (g cm<sup>-1</sup>), one calculates the adsorption rate constant  $k_1$  (s<sup>-1</sup>) of the gas adsorbate on the solid surface, together with its calibration factor of the detector  $g$  (cm/mol<sup>-1</sup> cm<sup>-3</sup>), and the diffusion coefficient of the adsorbate  $D_1$  (cm<sup>2</sup> s<sup>-1</sup>) in the carrier gas [9,10]. The above calculations can be

easily carried out by a relatively simple PC programme in GW-BASIC, already published as Appendix in [9,10], and also as Supporting Information to [3,5] available via the Internet.

The adsorption energy,  $\varepsilon$  (kJ mol<sup>-1</sup>), the local monolayer capacity,  $c_{\max}^*$  (mol g<sup>-1</sup>), the local isotherm value  $\theta_i$ , and the adsorption energy distribution function,  $f(\varepsilon)$  (mol<sup>2</sup> kJ<sup>-1</sup> g<sup>-1</sup>), mentioned in Section 1, are easily found from the values of  $A_i$ ,  $B_i$ ,  $v$ ,  $L_1$ ,  $a_y$ ,  $a_s$ ,  $k_1$ ,  $g$ ,  $D_1$ , as described elsewhere [3–6,10]. The various approximations used in the above calculations are stated in detail there, especially in [3–5]. Here only the equations needed for the lateral molecular interactions are briefly exposed.

First, two intermediate quantities,  $c_y$  (gaseous concentration above the solid at the end point of the solid bed in mol cm<sup>-3</sup>), and  $c_s^*$  (local adsorbed equilibrium concentration in mol g<sup>-1</sup> of the adsorbate) are given by the relations [10]:

$$c_y = \frac{vL_1}{gD_1} \sum_{i=1}^4 A_i \exp(B_i t) \quad (2)$$

$$c_s^* = \frac{a_y k_1 v L_1}{a_s g D_1} \sum_{i=1}^4 \frac{A_i}{B_i} [\exp(B_i t) - 1] \quad (3)$$

The desired energetic quantities  $\varepsilon$ ,  $c_{\max}^*$ ,  $\theta_i$  and  $f(\varepsilon)$ , mentioned before, are found from the derivatives  $\partial c_s^*/\partial t$ ,  $\partial c_s^*/\partial c_y$ ,  $\partial^2 c_s^*/\partial c_y^2$  and  $\partial^2 c_s^*/\partial c_y \partial t$ , previously published [3–5,10,11]:

$$\frac{\partial c_s^*}{\partial t} = \frac{a_y k_1 v L_1}{a_s g D_1} \sum_i A_i \exp(B_i t) = C_1 \quad (4)$$

$$\frac{\partial c_s^*}{\partial c_y} = \frac{a_y k_1 \sum_i A_i \exp(B_i t)}{a_s \sum_i A_i B_i \exp(B_i t)} = C_2 \quad (5)$$

$$\frac{\partial^2 c_s^*}{\partial c_y^2} = \frac{a_y k_1 g D_1}{a_s v L_1} \left\{ \frac{1}{\sum_i A_i B_i \exp(B_i t)} - \frac{\left[ \sum_i A_i \exp(B_i t) \right] \left[ \sum_i A_i B_i^2 \exp(B_i t) \right]}{\left[ \sum_i A_i B_i \exp(B_i t) \right]^3} \right\} = C_3 \quad (6)$$

$$\frac{\partial^2 c_s^*}{\partial c_y \partial t} = \frac{a_y k_1}{a_s} \left\{ 1 - \frac{\left[ \sum_i A_i \exp(B_i t) \right] \left[ \sum_i A_i B_i^2 \exp(B_i t) \right]}{\left[ \sum_i A_i B_i \exp(B_i t) \right]^2} \right\} = C_4 \quad (7)$$

Dividing Eq. (6) by Eq. (5), there results [3,10]

$$KRT = \frac{-C_3}{C_2} = RTK^0 \exp\left(\frac{\varepsilon}{RT}\right) \quad (8)$$

where  $K$  is Langmuir's constant,  $R$  is the gas constant and  $K^0$  is given by the relation

$$K^0 = \frac{h^3}{(2\pi m)^{3/2} (kT)^{5/2}} \quad (9)$$

$k$  being the Boltzmann's constant,  $m$  the molecular mass, and  $h$  the Planck's constant.

From Eq. (8), an obvious relation obtains the mean adsorption energy:

$$\varepsilon = RT[\ln(KRT) - \ln(RT) - \ln K^0] \quad (10)$$

The other adsorption quantities  $c_{\max}^*$  (local monolayer capacity),  $\theta_i$  (local adsorption isotherm) and  $f(\varepsilon)$  (old adsorption energy distribution function) are derived from Eqs. (3)–(8) above, as described in detail elsewhere [3–5,10]:

$$c_{\max}^* = c_s^* + \frac{C_2}{KRT} \quad (11)$$

$$\theta_i = \frac{c_s^*}{c_{\max}^*} = 1 - \frac{C_2}{c_{\max}^* KRT} \quad (12)$$

$$f(\varepsilon) = \frac{1}{RT} \left[ \frac{(KRT)C_1 + C_4}{\partial(KRT)/\partial t} - \frac{C_2}{KRT} \right] \quad (13)$$

It has been pointed out recently [11] that a combination of  $c_{\max}^*$ ,  $\theta_i$  and  $f(\varepsilon)$ :

$$\varphi(\varepsilon; t) = \frac{\theta_i f(\varepsilon)}{c_{\max}^*} \quad (14)$$

is a better choice for the true energy distribution

function, being an explicit function of the random variable  $\varepsilon$  and the structural parameter  $t$ . When  $\varphi(\varepsilon;t)$  is plotted [11] against  $\varepsilon$ , it has a purely Gaussian shape and can be normalised to unity with respect to the energy. If, however,  $\varphi(\varepsilon;t)$  is plotted against  $t$ , it gives in all systems studied [11] three probability bands. This was interpreted as showing three kinds of adsorption sites of different energy and relative population [11], according to the mechanism proposed by Bakaev and Steele [12] for the computer simulation of the argon adsorption on titanium dioxide. Obviously, this is not an arbitrary assumption but a conclusion based on experimental facts [11] like those of parts (b) in Figs. 1–3 here. Their calculations were based, among others, on the lateral interactions between adsorbed molecules. This gave us the inspiration to try the direct calculation of the lateral interaction energy from our experimental chromatographic data mentioned in the foregoing text. Such a calculation has never appeared in the literature, as far as we know.

One can start from the quantity  $KRT = -C_3/C_2$  calculated experimentally by means of Eq. (8), and showing that  $K = K^0 \exp(\varepsilon/RT)$ . This can be modified to include lateral interactions as

$$K' = K^0 \exp\left(\frac{\varepsilon}{RT} + \beta\theta_i\right) = K \exp(\beta\theta_i) \quad (15)$$

where  $\beta$  is a dimensionless parameter given by

$$\beta = \frac{z\omega}{RT} \quad (16)$$

$\omega$  being the lateral interaction energy and  $z$  the number of neighbours for each adsorption site. Thus,  $\theta_i z \omega$  is the added to  $\varepsilon$  differential energy of adsorption due to lateral interactions.

Our original starting point to derive Eqs. (8)–(14) was Jovanovic isotherm, critically analysed before [3]. It is also necessary here to incorporate in it the lateral interaction energy of Eq. (16), as follows:

$$\begin{aligned} \theta_i &= 1 - \exp(-K'p) = 1 - \exp[-Kp \exp(\beta\theta_i)] \\ &= 1 - \exp[-KRTc_y \exp(\beta\theta_i)] \end{aligned} \quad (17)$$

where the partial pressure  $p$  has been replaced by  $RTc_y$ , according to the ideal gas law. The partial

derivative  $\partial\theta_i/\partial c_y$  needed now can be obtained by writing Eq. (17) as a function of  $\theta_i$  and  $c_y$ ,  $F(\theta_i, c_y) = 0$ , and finding  $\partial\theta_i/\partial c_y = -(\partial F/\partial c_y)/(\partial F/\partial \theta_i)$ . The result is

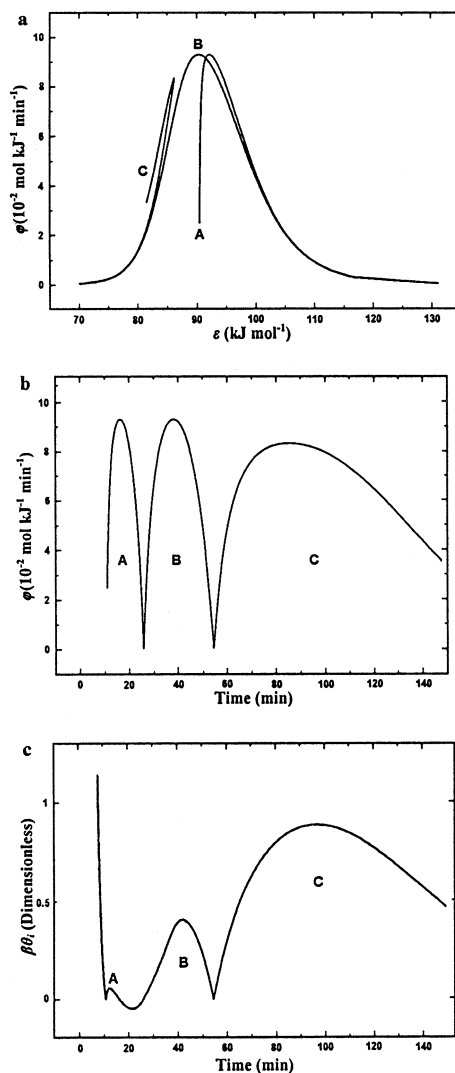


Fig. 1. Experimental behaviour of the adsorption energy distribution function and the lateral molecular interaction for the adsorption of 1-butene on cadmium sulphide, at 323.2 K. (a) The distribution function  $\varphi(\varepsilon;t)$ , as defined by Eq. (14), plotted against the adsorption energy  $\varepsilon$ . (b) The function  $\varphi(\varepsilon;t)$  plotted against the structural parameter of time  $t$ . (c) The lateral molecular interaction energy  $\beta\theta_i$  (dimensionless), defined by Eq. (15) and Eq. (16), plotted against the experimental time  $t$ .

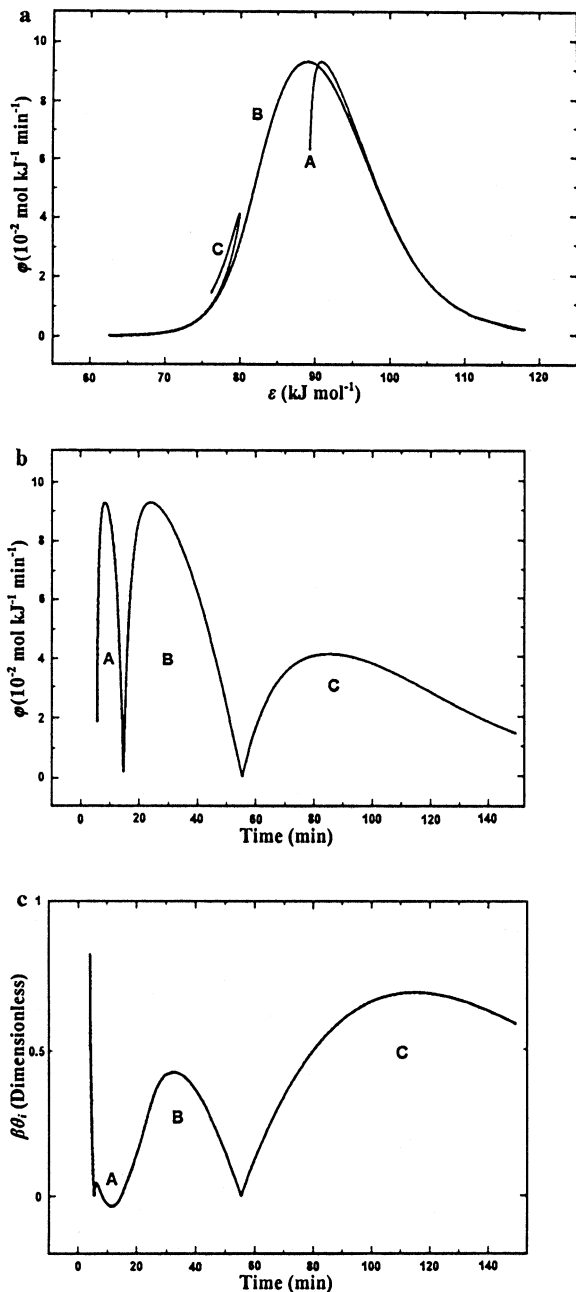


Fig. 2. Experimental behaviour of the adsorption energy distribution function and the lateral molecular interaction for the adsorption of ethane on calcium oxide, at 323.2 K. (a) The distribution function  $\varphi(\varepsilon;t)$ , as defined by Eq. (14), plotted against the adsorption energy  $\varepsilon$ . (b) The function  $\varphi(\varepsilon;t)$  plotted against the structural parameter of time  $t$ . (c) The lateral molecular interaction energy  $\beta\theta_i$  (dimensionless), defined by Eq. (15) and Eq. (16), plotted against the experimental time  $t$ .

$$\frac{\partial \theta_i}{\partial c_y} = \frac{KRT \exp(\beta\theta_i) \exp[-KRTc_y \exp(\beta\theta_i)]}{1 - KRTc_y \beta \exp(\beta\theta_i) \exp[-KRTc_y \exp(\beta\theta_i)]} \quad (18)$$

As a first approximation, we assume that  $\theta_i = 0$ , i.e. a bare surface. Then,  $\exp(\beta\theta_i) = 1$  and Eq. (18) simplifies to

$$\frac{1}{\partial \theta_i / \partial c_y} = \frac{\exp(KRTc_y)}{KRT} - \beta c_y \quad (19)$$

The left-hand side of the above equation can be calculated by inverting Eq. (11) of [3]. Substituting in that the Eq. (5) for  $\partial c_s^* / \partial c_y$  and the Eq. (11) for  $c_{\max}^*$ , one obtains

$$\frac{1}{\partial \theta_i / \partial c_y} = \frac{c_s^*}{C_2} + \frac{1}{KRT} \quad (20)$$

Thus, equating the right-hand sides of Eqs. (19) and (20), and solving for  $\beta$ , we obtain

$$\beta = \frac{1}{c_y} \left[ \frac{\exp(KRTc_y) - 1}{KRT} - \frac{c_s^*}{C_2} \right] \quad (21)$$

This is the first approximate calculation (for  $\theta_i = 0$ ) of the interaction parameter  $\beta$  of Eq. (16), obtained as a function of time, since all quantities on the right-hand side of Eq. (21) are known functions of time and can be calculated, namely,  $c_y$  by Eq. (2),  $KRT$  by Eq. (8),  $c_s^*$  by Eq. (3), and  $C_2$  by Eq. (5).

A second approximation of  $\beta$  can be found by correcting  $KRT$ , as calculated by Eq. (8) from  $C_2$  and  $C_3$ , through division by  $\exp(\beta\theta_i)$ , using the first approximation for  $\beta$  and the calculated  $\theta_i$  by means of Eq. (12). This correction is dictated by the definition (Eq. (15)), and can be repeated until the new calculated value of  $\beta$  differs from the previous one less than a chosen fraction of it, say 0.1.

#### 4. Results and discussion

By entering the pair values of  $H$ ,  $t$  into the 3000–3040 DATA lines of the GW-BASIC pro-

gramme given in the Supporting Information of [3,5] or in the Appendix of [10], together with the other known quantities needed in the INPUT lines, one obtains the values of  $\varepsilon$ ,  $c_{\max}^*$ ,  $\theta_i$  and  $f(\varepsilon)$  as a function of chosen times. The following additional lines can be added to the PC programme of [10] to obtain simultaneously the function  $\varphi(\varepsilon; t)$  of Eq. (14), as well as the values of  $\beta$  being calculated by means of Eq. (21), again as a

function of chosen times. The new complete GW-BASIC programme is available from the corresponding author.

Some representative results are given in Figs. 1–3, where the time profile of the dimensionless lateral interaction energy  $\beta\theta_i$ , introduced by Eq. (15) and Eq. (16), is shown in parallel with the energy distribution function  $\varphi(\varepsilon; t)$ , plotted against  $\varepsilon$  and  $t$ .

```

3420 LPRINT TAB(1);"T";TAB(7);"E";TAB(17);"Cs";TAB(27);"Theta";TAB(40);"Phi";
      TAB(50);"100Beta*Theta"
3425 LPRINT TAB(1);"(min)";TAB(7);"(kJ/mol)";TAB(15);"(micromol/g)";TAB(35);
      "(centimol/kJ min)";TAB(50);"(dimensionless)"
3591 PHI=THETA*FE/CSMAX
3592 COUNT=1
3593 BETA1=((EXP(KRT*CY)-1)/KRT-CS*ABBT/M1/ABT)/CY
3594 KRT1=KRT/EXP(BETA1*THETA)
3595 BETA2=((EXP(KRT1*CY)-1)/KRT1-CS*ABBT/M1/ABT)/CY
3596 IF ABS(BETA2-BETA1)<.1*BETA1 GOTO 3600
3597 BETA1=BETA2:COUNT=COUNT+1:IF COUNT>5 GOTO 3600
3598 GOTO 3594

3600 LPRINT TAB(1);T;TAB(5);E1/1000;TAB(15);CS*10^6;TAB(26);THETA;
      TAB(35);PHI*100;TAB(50);BETA2*THETA*100

```

Table 1

Characteristics of the plots of the energy distribution function  $\varphi(\varepsilon; t)$  against time at 323.2 K in the first two gas/solid systems, and 333.2 K for the last system

Gas/solid	Time of maxima (min)			Energy of maxima (kJ mol <sup>-1</sup> )			Time of minima (min)		% Curve areas		
	$t_A$	$t_B$	$t_C$	$\varepsilon_A$	$\varepsilon_B$	$\varepsilon_C$	$t_{AB}$	$t_{BC}$	A	B	C
1-C <sub>4</sub> H <sub>8</sub> /CdS	16.4	38.2	85.2	92.2	90.4	86.2	25.9	54.4	11.48	20.84	67.68
C <sub>2</sub> H <sub>6</sub> /CaO	8.2	24.0	85.2	90.8	89.0	80.0	14.7	55.4	10.52	42.28	47.20
trans-2-C <sub>4</sub> H <sub>8</sub> /CaCO <sub>3</sub>	24.1	52.6	124.7	91.6	89.3	79.4	35.7	92.4	23.79	62.05	14.16

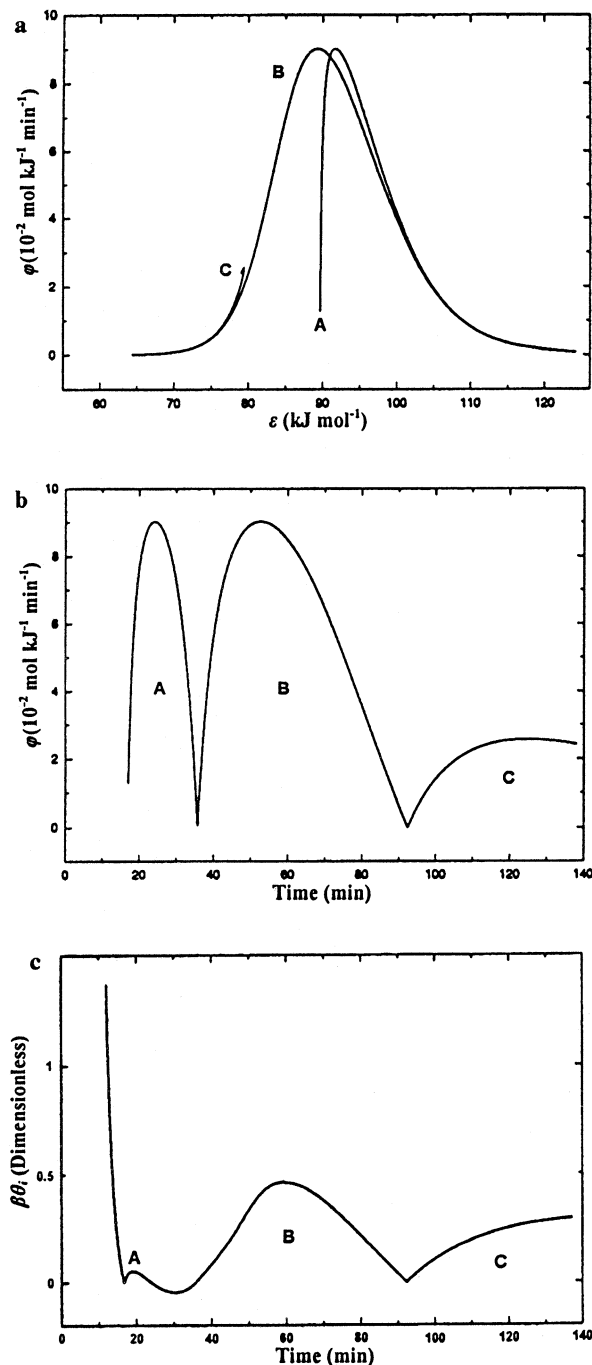


Fig. 3

The model of Bakaev and Steele [12], based on the computer simulation of the argon adsorption on titanium dioxide, can be adopted again. It uses

the assumption that, after filling some (or all) minima of adsorption potential, the adsorbed molecules create new adsorption sites by providing support to new molecules held at positions which were initially local maxima (saddle points) of the surface. This support to molecules interacting weakly with the surface is due to favourable lateral interactions with the neighbouring adsorbate molecules, thus enhancing the overall probability of adsorption and facilitating completion of the first monolayer. Finally, a third kind of adsorption with smaller energy was attributed to molecules very loosely bound to the substrate, in its second layer. This layer begins to grow when the first layer is almost totally completed and serves as a surface of adsorbent for the second layer. The above three steps of the adsorption mechanism of Bakaev and Steele [12], based only on computer simulated results, are strongly supported by the present experimental results. Parts A of the plots in Figs. 1–3 follow the adsorption at potential minima appearing early in time. Parts B are due to the new adsorption sites created later by lateral interactions with previously adsorbed molecules. And parts C are attributed to adsorption on the second layer.

Although the three Figures describe the experimental behaviour of three different hydrocarbons adsorbing on three quite different solid surfaces, the appearance of all curves is quite similar. The same applies to other systems. In Table 1, the characteristics of the plots in Fig. 1(b), Fig. 2(b), Fig. 3(b) are listed.

It is worth noting that the three maxima and the two minima in Fig. 1(b), Fig. 2(b), Fig. 3(b) almost coincide in time with the three maxima and the two minima of Fig. 1(c), Fig. 2(c), Fig. 3(c), respectively. This points to a probable connection between them, adding a further support to the mechanism of Bakaev and Steele [12]. The relative areas under the

Fig. 3. Experimental behaviour of the adsorption energy distribution function and the lateral molecular interaction for the adsorption of *trans*-2-butene on Penteli marble, at 333.2 K. (a) The distribution function  $\phi(\epsilon;t)$ , as defined by Eq. (14), plotted against the adsorption energy  $\epsilon$ . (b) The function  $\phi(\epsilon;t)$  plotted against the structural parameter of time  $t$ . (c) The lateral molecular interaction energy  $\beta\theta_i$  (dimensionless), defined by Eq. (15) and Eq. (16), plotted against the experimental time  $t$ .

curves A, B and C of the plots in Fig. 1(b), Fig. 2(b), Fig. 3(b) are given in Table 1. These areas obviously represent the relative quantities of the adsorbate gas in the three adsorption states.

### Acknowledgements

The authors thank Anna Malliori for typing the manuscript.

### References

- [1] M. Jaroniec, R. Madey, *Physical Adsorption on Heterogeneous Solids*, Elsevier, Amsterdam, 1988.
- [2] W. Rudzinski, D.H. Everett, *Adsorption of Gases on Heterogeneous Surfaces*, Academic, New York, 1992.
- [3] N.A. Katsanos, E. Arvanitopoulou, F. Roubani-Kalantzopoulou, A. Kalantzopoulos, *J. Phys. Chem. B* 103 (1999) 1152.
- [4] N.A. Katsanos, N. Rakintzis, F. Roubani-Kalantzopoulou, E. Arvanitopoulou, A. Kalantzopoulos, *J. Chromatogr. A* 845 (1999) 103.
- [5] N.A. Katsanos, E. Iliopoulou, F. Roubani-Kalantzopoulou, E. Kalogirou, *J. Phys. Chem. B* 103 (1999) 10228.
- [6] C. Abatzoglou, N.A. Katsanos, A. Kalantzopoulos, F. Roubani-Kalantzopoulou, *Stud. Surf. Sci. Catal.* 122 (1999) 175.
- [7] N.A. Katsanos, *Flow Perturbation Gas Chromatography*, Marcel Dekker, New York, 1988.
- [8] C. Abatzoglou, E. Iliopoulou, N.A. Katsanos, F. Roubani-Kalantzopoulou, A. Kalantzopoulos, *J. Chromatogr. A* 775 (1997) 211.
- [9] N.A. Katsanos, R. Thede, F. Roubani-Kalantzopoulou, *J. Chromatogr. A* 795 (1998) 133.
- [10] N.A. Katsanos, F. Roubani-Kalantzopoulou, *Adv. Chromatogr.* 40 (2000) 231.
- [11] F. Roubani-Kalantzopoulou, T. Artemiadi, I. Bassiotis, N.A. Katsanos, V. Plagianakos, *Chromatographia* 53 (2001) 315.
- [12] V.A. Bakaev, W.A. Steele, *Langmuir* 8 (1992) 1372.
- [13] N.A. Katsanos, E. Dalas, *J. Phys. Chem.* 91 (1987) 3103.